High-resolution crystal structure of the non-specific lipid-transfer protein from maize seedlings

Dong Hae Shin, Jae Young Lee, Kwang Yeon Hwang, Kyeong Kyu Kim and Se Won Suh*

Department of Chemistry, College of Natural Sciences, Seoul National University, Seoul 151-742, Korea

Background: The movement of lipids between membranes is aided by lipid-transfer proteins (LTPs). Some LTPs exhibit broad specificity, transferring many classes of lipids, and are termed non-specific LTPs (ns-LTPs). Despite their apparently similar mode of action, no sequence homology exists between mammalian and plant ns-LTPs and no three-dimensional structure has been reported for any plant ns-LTP.

Results: We have determined the crystal structure of ns-LTP from maize seedlings by multiple isomorphous replacement and refined the structure to 1.9 Å resolution. The protein comprises a single compact domain with four α-helices and a long C-terminal region. The eight conserved cysteines form four disulfide bridges (assigned as Cys4–Cys52, Cys14–Cys29, Cys30–Cys75, and Cys50–Cys89) resolving the ambiguity that remained from the chemical determination of pairings in the homologous protein from castor bean. Two of the bonds, Cys4–Cys52 and Cys50–Cys89, differ from what would have been predicted from sequence alignment with soybean hydrophobic protein. The complex between maize ns-LTP and hexadecanoate (palmitate) has also been crystallized and its structure refined to 1.8 Å resolution.

Conclusions: The fold of maize ns-LTP places it in a new category of all-α-type structure, first described for soybean hydrophobic protein. In the absence of a bound ligand, the protein has a tunnel-like hydrophobic cavity, which is large enough to accommodate a long fatty acyl chain. In the structure of the complex with palmitate, most of the acyl chain is buried inside this hydrophobic cavity.

Structure 15 February 1995, **3**:189–199
Key words: lipid-transfer protein, maize protein, X-ray structure

Introduction

Lipid-transfer proteins (LTPs), responsible in part for the movement of phospholipids, glycolipids, fatty acids and sterols between membranes, are widely distributed among eukaryotic and prokaryotic cells [1]. Some of these proteins show narrow substrate specificities, whereas others are non-specific [2]. The amino acid sequences of several non-specific lipid-transfer proteins (ns-LTPs) from animal and plant sources have been reported [3–7]. The mammalian ns-LTPs have in general a molecular weight of 12–14 kDa and a pI in the range 8.6–9.6, except for the rat hepatoma ns-LTP, which has an acidic pI [8].

Despite their apparently similar mode of action, plant ns-LTPs have a smaller molecular weight (~9 kDa) and exhibit no sequence homology with mammalian ns-LTPs. However, sequence similarity among plant ns-LTPs is high and they have in general eight conserved cysteine residues, which form four disulfide bonds [9]. The sequences of several small plant proteins including amylase inhibitor I-2 from the seeds of ragi, Indian finger millet [9,10], and probable amylase/protease inhibitors from barley and rice [11,12] are also similar to those of ns-LTPs. The sequence identity between the maize ns-LTP and barley protein is ~52% and that between the maize and ragi proteins 67% [9]. As plant ns-LTPs also bind strongly to fatty acids and acyl-coenzyme A (acyl-CoA), they have been proposed to function as fatty acid and acyl-CoA binding proteins [13–16]. A defensive role for plant ns-LTPs against bacterial and fungal pathogens has also been proposed [17].

The tertiary structure of plant ns-LTPs was proposed to consist of mainly β-sheets on the basis of primary sequences of several ns-LTPs [6]. However, recent studies of wheat ns-LTP by NMR [18], infrared and Raman spectroscopy [7] showed that the polypeptide chain appears to be organized mainly as helical segments connected by disulfide bridges and that the helical structure is essential for the transfer activity. However, no three-dimensional structure of any plant ns-LTP has been reported.

Ns-LTP from maize seedlings is a small basic protein consisting of 93 amino acid residues with a molecular weight of 9055 Da [6]. It transfers phospholipids such as phosphatidylcholine, phosphatidylethanolamine and phosphatidylinositol *in vitro* [6]. The crystallization and preliminary X-ray crystallographic characterization of this protein have been reported [19]. Here, we present the structure of uncomplexed maize ns-LTP, which has been determined by the multiple isomorphous replacement (MIR) method of X-ray crystallography and refined against 1.9 Å data. We also report the structure of ns-LTP in complex with palmitate, refined at 1.8 Å resolution.

*Corresponding author.

Results and discussion

Overall structure of uncomplexed ns-LTP

The present model of uncomplexed maize ns-LTP has been refined at 1.9 Å to an R-factor of 19.9% (no sigma cutoff), with root mean square (rms) deviations from ideality of 0.016 Å and 1.98° for bond lengths and bond angles, respectively. Therefore, the overall structure is highly reliable. However, six residues (Ala1, Ile2, Gln21, Gly22, Ile79 and Pro80) are only poorly defined by the electron-density maps. The maize ns-LTP is composed of a single compact domain with approximate dimensions of 37 Å×26 Å×23 Å, as shown in Fig. 1a. A Cα trace of the polypeptide backbone is shown in Fig. 1b. For the convenience of discussion, the structure may be divided into three segments, the first comprising four α-helices [H1 (residues 4–18), H2 (residues 27–39), H3 (residues 43–58), H4 (residues 65–75)]; the second including three short loops connecting these α-helices [L1 (residues 19–26), L2 (residues 40–42), L3 (residues 59–64)]; and the third being the long C-terminal region (residues 76–93) (Fig. 1a). The protein lacks any β-structure and nearly two-thirds of its residues are found in α-helices. Thus it should be classified as an all-α structure [20]. Its folding pattern is, however, distinctive among α-helical globular proteins, with the fold belonging to a new category, first discovered in a hydrophobic protein from soybean (HPS) [21,22]. Previously, a tentative tertiary structure model of maize ns-LTP was proposed that consisted mainly of β-sheets [6], but this is clearly wrong. The present assignment of α-helices in maize ns-LTP in the crystalline state agrees in the main with the result of an NMR study of wheat ns-LTPs in solution [18].

The first α-helix (H1) is significantly bent at the Pro13 residue and can be divided into two parts, H1a and H1b comprising two turns and one turn respectively (Fig. 1a). The NMR study on wheat ns-LTP also indicated a bend at Pro13. The last helix (H4) is also slightly bent by the presence of Pro72 at the beginning of the last turn (Fig. 1a). The long C-terminal region contains one turn of 3_{10}-helix, residues 89–91 (Figs 1a and 1b).

Disulfide bonds

Two clusters of disulfide bonds are located on the two opposing sides of the structure (Fig. 2a). Both N-terminal and C-terminal regions of the protein are linked to the long α-helix, helix H3, by a pair of disulfide bonds, Cys4–Cys52 and Cys50–Cys89 (Fig. 2a). The other pair, Cys14–Cys29 and Cys30–Cys75, link the ends of α-helices H1b and H4 to the N terminus of another long α-helix, helix H2. This assignment of four disulfide bridges on the basis of the refined X-ray structure not only confirms the previous chemical determination on a homologous ns-LTP from castor bean [4], but also resolves the ambiguity which remained. Two disulfide

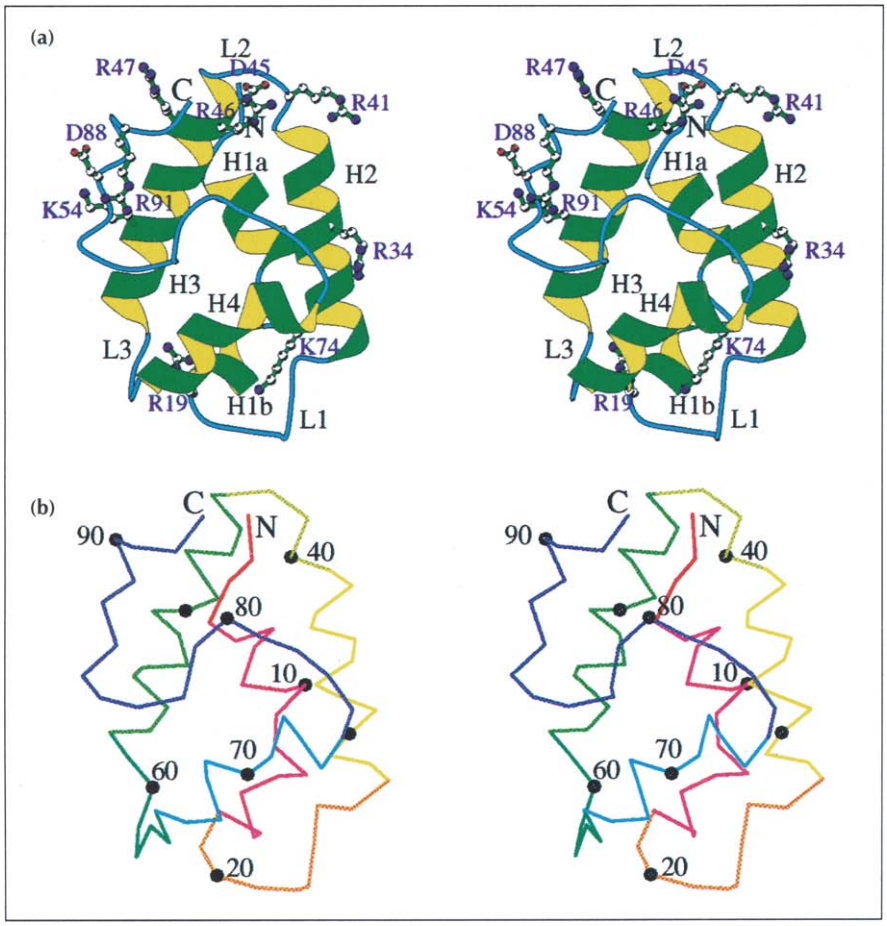

Fig. 1. **(a)** Stereo ribbon diagram of maize non-specific lipid-transfer protein (ns-LTP) (drawn with MOLSCRIPT [47]). The N and C termini are indicated as are eight basic and two acidic residues. Secondary structure was assigned with PROCHECK [48]. **(b)** Stereo drawing of the Cα trace of maize ns-LTP. Every tenth residue is labeled and the segments in the structure are colored as follows: N-terminal region and H1, red; L1, orange; H2, yellow; L2, pale green; H3, green; L3, dark green; H4, cyan; C-terminal region, dark blue.

bonds, Cys4–Cys52 and Cys50–Cys89, agree with the previous chemical determination on castor bean ns-LTP [4], but the exact pairing between Cys29, Cys30 and Cys14, Cys75 was not known [4]. The present assignment of Cys14–Cys29 and Cys30–Cys75, as shown in Fig. 2b, resolves the ambiguity and is also consistent with the observation of nuclear Overhauser effects in the NMR study of wheat ns-LTP [18]. However, the pairings Cys4–Cys52 and Cys50–Cys89 differ from what might have been predicted on the basis of an alignment of the conserved cysteine residues in HPS and maize ns-LTP [21] (Fig. 3).

Distribution of polar and non-polar residues in the uncomplexed structure

Maize ns-LTP has three negative and nine positive charges at neutral pH. Besides the charges of the N-terminal amino and C-terminal carboxylate groups, there are two aspartates (Asp45, Asp88), six arginines (Arg19, Arg34, Arg41, Arg46, Arg47, Arg91), and two lysines (Lys54, Lys74). All three negative charges are located on one side of the protein (Fig. 4). Two positively charged residues, Arg19 and Arg41, are poorly conserved in proteins of similar sequence. The electron densities of the charged groups are well defined except for the N-terminal amino group and side-chain atoms of three of the arginines (Arg19, Arg41, Arg91). Except for Arg91, all the charged groups are involved in either salt bridges or hydrogen bonds within a single polypeptide chain. The N-terminal amino group interacts with Asp45 (Ala1 N...Oδ2 Asp45: 3.8 Å) and the C-terminal asparagine interacts with Arg46 (Arg46 Nη2...Oδ1 Asn93: 2.4 Å). The following strong or weak hydrogen-bond interactions between the positively charged residues and the backbone carbonyl oxygen atoms provide further stabilization for the tertiary fold: (Arg19 Nη2...O Gly59: 3.6 Å), (Arg34 Nη2...O Cys75: 2.6 Å), (Arg34 Nη2...O Gly76: 3.6 Å), (Arg47 Nη2...O Ser90: 3.8 Å), (Arg47 Nη2...O Val92: 3.3 Å) and (Lys54 Nζ...O Thr87: 2.8 Å). There is also a hydrogen bond between the side chain of Lys74 and the Tyr17 hydroxyl (Lys74 Nζ...Oη Tyr17: 3.0 Å). Other intramolecular hydrogen-bond interactions involving charged residues are as follows: (Arg41 Nη1...O Asn38: 2.7 Å) and (Asp88 Oδ2...Oγ Ser90: 3.5 Å). It is interesting to note that the distribution of the charges on the surface of the maize ns-LTP structure is highly non-uniform (Fig. 4). The charges are clustered around the C terminus, except for Arg19 (which is not well conserved), and Arg34 and Lys74 (which are clustered near the N terminus of the long C-terminal region) (Fig. 4). The uneven charge distribution may contribute to the attraction of the negatively charged groups in fatty acids and phospholipids (Fig. 5).

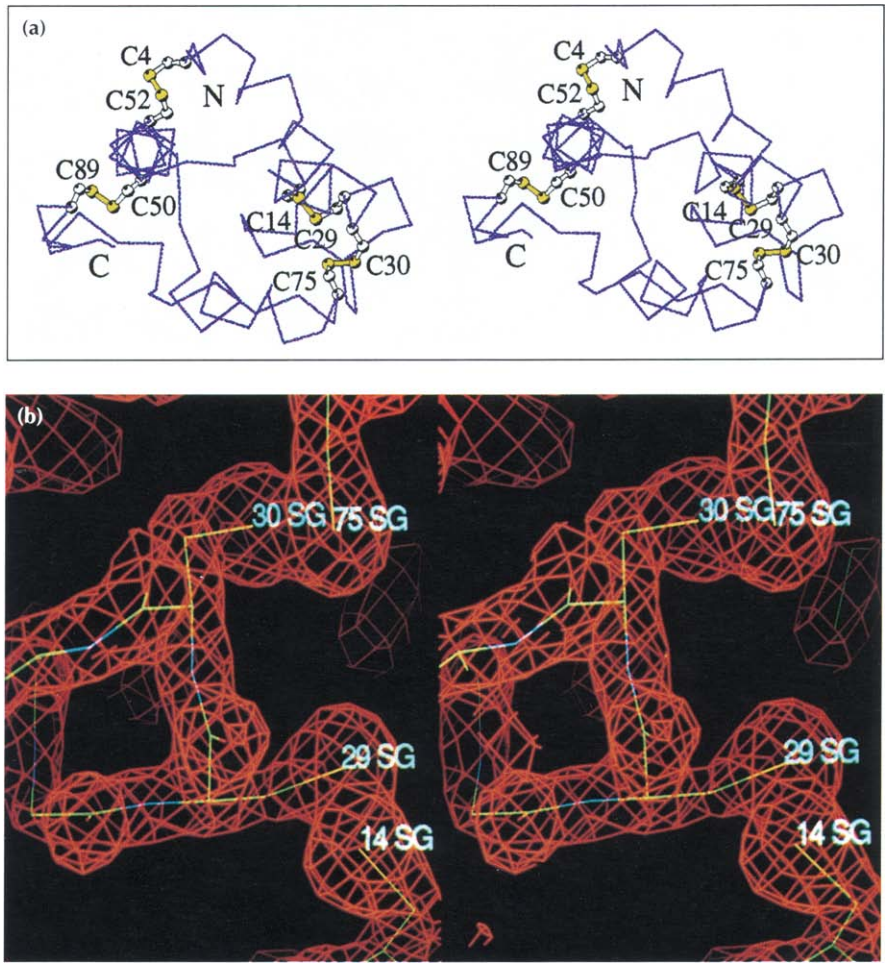

Fig. 2. (a) Stereo diagram showing four disulfide bridges viewed along the axis of α-helix H3. Sulfur atoms are colored yellow. (Drawn with MOLSCRIPT [47].) **(b)** Stereo diagram of the $2F_o–F_c$ map around the Cys14–Cys29 and Cys30–Cys75 disulfide bridges. The map is calculated using all reflections between 8 Å and 1.9 Å and contoured at 1.5σ. (Figure drawn using the program CHAIN [49].)

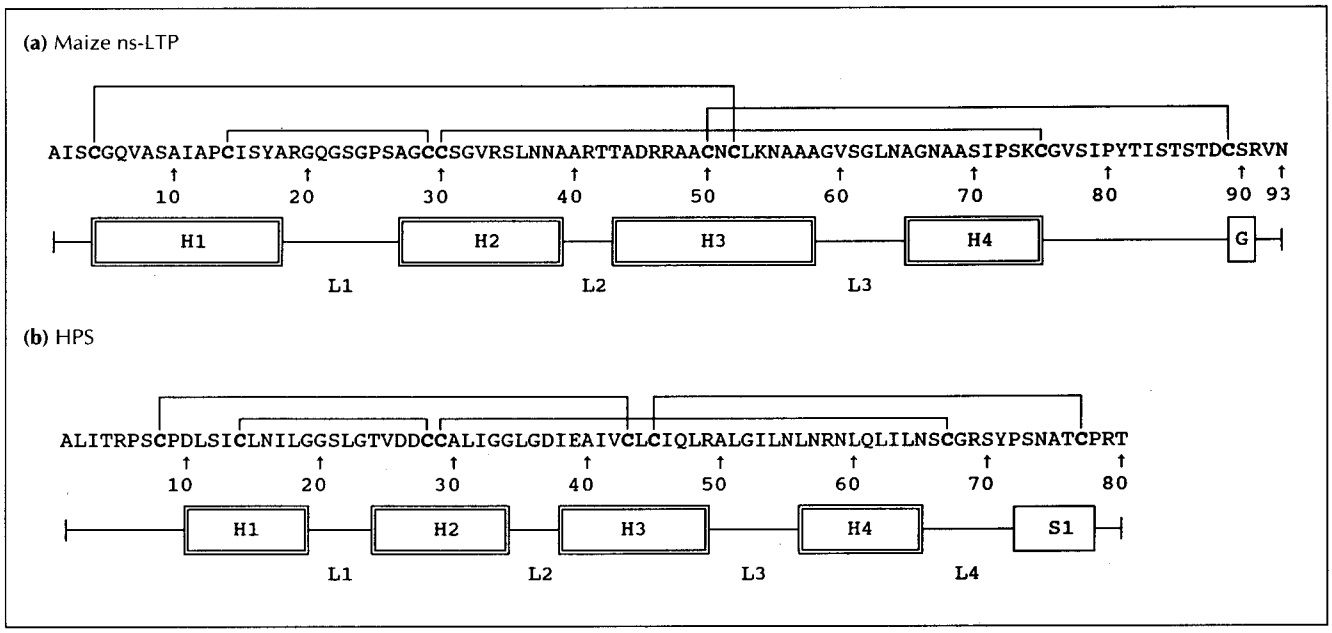

Fig. 3. Comparison of disulfide bridge patterns and secondary structures of maize ns-LTP **(a)** and hydrophobic protein from soybean **(b)**. H, α-helix; G, 3_{10}-helix; S, β-strand; L, loop.

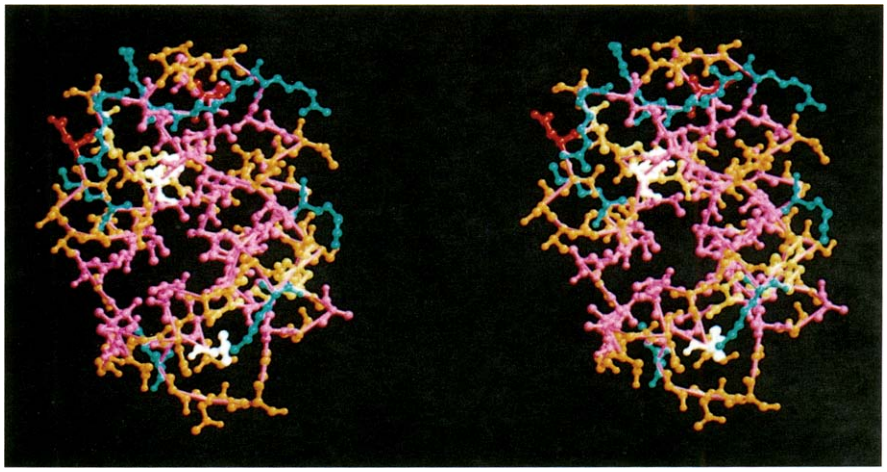

Fig. 4. Stereo diagram showing the amino acid distribution in uncomplexed maize ns-LTP. Basic residues (Arg, Lys) are colored cyan; acidic residues (Asp), red; neutral polar residues (Asn, Gln, Gly, Ser, Thr), orange; Tyr, white; hydrophobic residues (Ala, Ile, Leu, Pro, Val), pink; Cys, yellow.

All of the side chains in 28 neutral polar residues (asparagine, glutamine, serine and threonine) are located on the protein surface. Two tyrosines (Tyr17 and Tyr81) are half-exposed (Fig. 4). The terminal oxygen atom of Tyr17 points towards the bulk solvent, whereas the side chain of Tyr81 points into a solvent channel in its vicinity. Among the 10 glycines in this protein, five are contained within the two loops (L1 and L3). The side-chain atoms of 35 hydrophobic residues (alanine, valine, isoleucine, leucine and proline) are largely buried inside the protein (Fig. 4), defining the surface of a tunnel-like hydrophobic cavity, as discussed below.

The tunnel-like hydrophobic cavity and the binding of fatty acids

One of the most interesting features in the structure of uncomplexed maize ns-LTP is the presence of a tunnel-like hydrophobic cavity, which runs through the protein, from one end near residue Ala40, to the other near Ala18. The tunnel-like hydrophobic cavity has an approximate diameter of 5 Å and a length of 15 Å as defined by the van der Waals surface of the tunnel atoms. This hydrophobic cavity is somewhat curved. Its length is sufficient to accommodate ~12 carbon atoms in a single acyl chain of long fatty acids. Roughly speaking, the tunnel is formed by placing part of the long C-terminal region (residues 77–83) over the hydrophobic channel, whose hydrophobic surface is provided by the buried side-chain atoms of the four amphipathic α-helices, H1 to H4. The C-terminal region does not cover the hydrophobic channel completely, so there is a small gap (~2 Å wide and 12 Å long), in which five water molecules are bound to the backbone atoms by a network of hydrogen bonds.

All ordered water molecules are found on the surface of the molecule and there is no evidence from the electron density for any ordered water molecules inside the

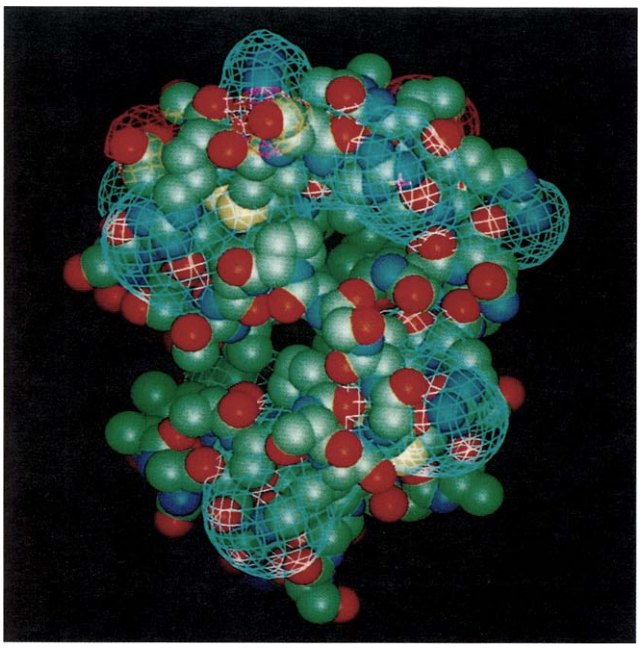

Fig. 5. Electrostatic potential map calculated for the uncomplexed maize ns-LTP. The DELPHI program (Biosym, San Diego, California, USA) was used to calculate an approximate solution to the linearized Poisson–Boltzmann equation. Only formal protein charges were included in the calculation. Positive (cyan) and negative (red) contours in the potential are evaluated at +2 kT/e$^-$ and −2 kT/e$^-$, respectively.

hydrophobic cavity. The tunnel-like hydrophobic cavity of the uncomplexed ns-LTP is probably filled with disordered solvent molecules, as it is difficult to have an evacuated volume of this magnitude inside a protein. Hence the present structure of uncomplexed maize ns-LTP does not have a tightly packed hydrophobic core, which is typically found in many globular, water-soluble proteins. It seems that the disulfide bonds and charge interactions including hydrogen bonds, as discussed above, play important roles in maintaining the tertiary structure of this protein in the absence of a bound ligand. Because of the presence of the tunnel-like hydrophobic cavity, the interactions among hydrophobic side chains of the four α-helices are either absent or rather limited. No interaction exists between the hydrophobic side chains of two α-helices in the pairs H4–H1 and H4–H3, and one interaction is present in the helical pairs H4–H2 (Ile71 Cγ1...Cγ2 Val33: 4.0 Å) and H2–H3 (Leu53 Cδ1...Cδ2 Leu36: 4.2 Å). A few hydrophobic side-chain interactions exist between the two α-helices in the helical pairs H1–H2 [(Val7 Cγ2...Cδ1 Leu36: 3.7 Å), (Ala10 Cβ...Cδ1 Leu36: 4.4 Å), (Ile11 Cδ1...Cγ2 Val33: 3.7 Å)] and H1–H3 [(Val7 Cγ1...Cδ2 Leu53: 3.5 Å), (Ile11 Cγ1...Cδ2 Leu53: 3.9 Å)].

The majority of the residues in this protein (at least 75%) seem to be indispensable for maintaining the shape of the hydrophobic cavity. Therefore, the present structure of maize ns-LTP provides an excellent example of a highly economical protein design for a given function. The inner surface of the hydrophobic cavity is formed by the side-chain carbon atoms of the following amino acid residues: Ile11, Ser14, Ile15 and Ala18 of helix H1; Val33, Leu36 of helix H2; Ala40 of loop L2; Ala49, Leu53, Ala56 and Ala57 of helix H3; Val60 and Leu63 of loop L3; Ala68, Ile71 and Pro72 of helix H4 and Val77, Ile79 and Ile83 in the C-terminal region. The B-factors of residues 78–81 are the highest (Fig. 6a), with the exception of the two N-terminal residues, which show only weak electron density and are probably disordered. The apparent flexibility of the region from 78–81, together with its location near the wider mouth (see below) of the tunnel-like hydrophobic cavity suggests a possible role in binding and subsequent release of fatty acids and phospholipids.

If the hydrophobic cavity is viewed as roughly tunnel-shaped, one end of the hydrophobic tunnel, near Ala40, has an opening ~5 Å in diameter and this can conceivably be a part of the entrance or exit for the acyl chain of fatty acids or phospholipids. Some of the polar and charged residues in the vicinity of this tunnel opening can make favorable interactions with the polar moieties of fatty acids or phospholipids. On the other hand, the other end of the tunnel, near Ala18, has a narrower opening with a diameter of ~3 Å and only non-polar residues are found nearby. It is unlikely that this end

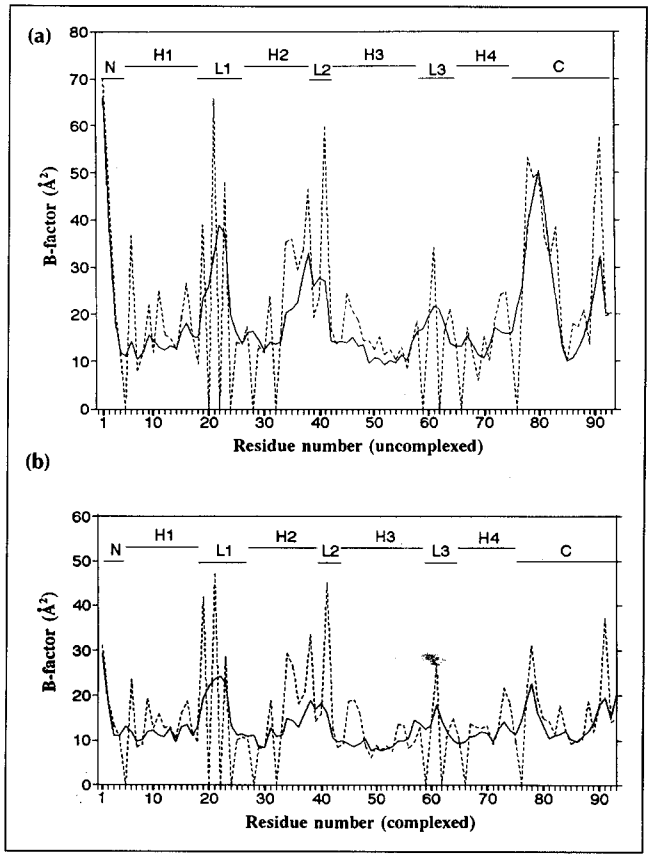

Fig. 6. B-factor plot of maize ns-LTP. **(a)** Uncomplexed and **(b)** complexed models. Average B-factors for the main-chain atoms (solid lines) and side-chain atoms (dashed lines) in the uncomplexed model are 19.1 Å^2 and 23.5 Å^2, respectively. Those in the complexed model are 12.7 Å^2 and 18.0 Å^2.

serves as the main entrance or exit for the fatty acyl chain because it has a narrower aperture and seems to have only a limited flexibility, as suggested by the low B-factors (residues 83–85 and 57–68; see Fig. 6a). A narrow gap, ~2 Å wide and 12 Å long, between a part of the C-terminal region and the α-helix H4 could possibly play a role in binding and releasing of a fatty acid. It is also conceivable that a conformational change involving the movement of the flexible region (residues 78–81) and a rearrangement of structural elements could occur during the binding and releasing of fatty acid.

Small plant proteins having similar molecular weights and pI values to maize ns-LTP have been shown to bind strongly to fatty acids and acyl-CoA, whereas only weak binding of phosphatidylcholine was observed [14,15]. A dissociation constant of 3.5×10^{-6} M has been reported for the binding of oleic acid by an LTP-like basic protein from oat [13]. A 1:1 stoichiometry of binding of fatty acid by a plant ns-LTP was indicated by the previous biochemical data [15,16]. Neither the binding stoichiometry nor the binding constant for any phospholipid has been reported in the literature. The volume of the hydrophobic cavity, which is only loosely defined, is estimated to be ~300 $Å^3$ by the program VOIDOO [23], whereas that of the 12-carbon hydrocarbon chain is 215 $Å^3$. The discrepancy is explained by the fact that the surface of the hydrophobic cavity is not exactly complementary to the molecular surface of the hydrocarbon chain, as revealed by the structure of the complex with palmitate (see below).

Binding of palmitate and structural changes in ns-LTP

In order to provide a more detailed picture of the interactions between the bound ligand and protein, the structure of maize ns-LTP in complex with palmitate has been refined at 1.78 Å resolution to an R-factor of 19.3% (no sigma cutoff) with rms deviations from ideality of 0.016 Å and 1.78° for bond lengths and bond angles, respectively. All 93 residues in the complex model are well defined in the electron-density maps, except for side-chain atoms of Gln21, Arg41 and Arg91. Average B-factors of the complex structure are somewhat lower than that of the uncomplexed model (Fig. 6b). The model of the complex with the bound ligand and some solvent molecules is shown in Fig. 7a and the CPK model of ns-LTP with the bound palmitate is presented in Fig. 7b. The overall fold of the complex with palmitate (shown in white in Fig. 7a) is identical to that of the uncomplexed structure (cyan in Fig. 7a), and the two structures show only small differences, except in a few places (Fig. 7a). A comparison of the two structures gives an rms difference of 0.79 Å for all 625 atoms in the 93 residues (Fig. 8). For 372 main-chain atoms the rms difference is 0.54 Å and for 253 side-chain atoms it is 0.96 Å. Other than the two N-terminal residues, which are probably disordered and thus poorly defined in the uncomplexed model, the residues exhibiting rms differences >1.0 Å are in the C-terminal region, between residues 79 and 85 (Fig. 8).

The shift of the backbone in the C-terminal region results in a slight swelling of the tunnel-like hydrophobic cavity in the complex structure (Fig. 7a). The B-factors in this region are very high in the uncomplexed structure relative to the complexed structure (compare Fig. 6a and Fig. 6b). In agreement with this, the two residues Ile79 and Pro80, which are only poorly defined in the uncomplexed model, show well defined electron densities in the complexed model. The side-chain atoms of three isoleucine residues (Ile11, Ile79 and Ile83) which define the surface of the tunnel-like hydrophobic cavity show large rms differences, above 2.3 Å (Fig. 8). In the complex structure, these side-chain atoms are displaced from the hydrophobic cavity so that the acyl chain of

Fig. 7. **(a)** Stereo diagram showing the structural comparison of maize ns-LTP in the presence and absence of palmitate. The backbone trace of uncomplexed (cyan) and complexed (white) proteins are shown overlaid. The bound palmitate is shown in green for carbon atoms and red for oxygen atoms. Seven ordered water molecules, which are located in the gap between a part of the C-terminal region and the helix H4, are shown as red spheres. **(b)** CPK representation of maize ns-LTP in complex with palmitate. Palmitate is colored green and amino acid residues are colored according to type as in Fig. 4.

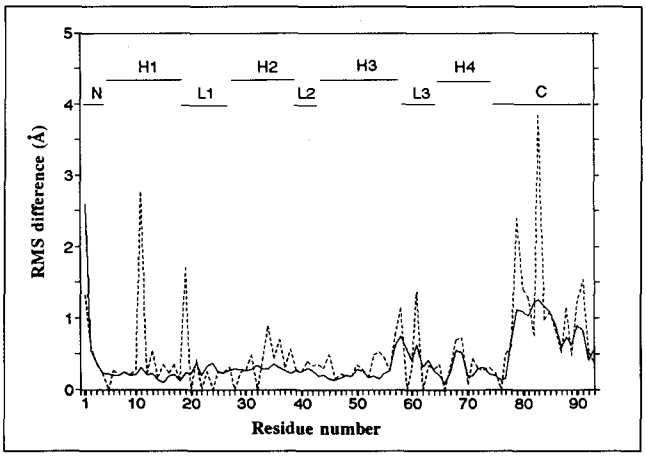

Fig. 8. Comparison of uncomplexed and complexed ns-LTP structures. Rms differences for the main-chain atoms (solid lines) and side-chain atoms (dashed lines) of each residue are plotted.

palmitate fits comfortably inside the hydrophobic cavity without bad contacts. The following hydrophobic residues contribute to the interaction of the fatty acid tail with the protein: Ile11, Ile15 and Ala18 of helix H1; Val33 and Leu36 of helix H2; Ala40 of loop L2; Ala49 and Leu53 of helix H3; Val60 of loop L3; Ile71 and Pro72 of helix H4; and Val77 and Ile 79 in the C-terminal region (Table 1). Other residues that contribute to the surface of the tunnel-like hydrophobic cavity do not make close contacts with the fatty acid, because the surface of the hydrophobic cavity is not smooth. A small, elongated gap between the C-terminal region and the α-helix H4 is clearly seen in Fig. 7b. In this gap, seven water molecules are bound to the backbone atoms by a network of hydrogen bonds (Fig. 7a), whereas only five water molecules are seen in the corresponding gap of the uncomplexed structure. In the complexed structure, one of these waters, Sol117, is within 4.5 Å of the hydrocarbon chain of palmitate (Table 1).

The carboxylate group of the bound palmitate is exposed to solvent, whereas ~12 carbon atoms in the tail of the palmitate chain can be considered to be buried inside the tunnel-like hydrophobic cavity (Figs 7a and 7b). Oxygen atoms of the carboxylate group form hydrogen bonds with the hydroxyl group of Tyr81 and two bound water molecules (Sol152 and Sol197; see Table 1). Table 1 lists the torsion angles of bound palmitate as well as the temperature factors for each atom. Comparison with the uncomplexed structure reveals that there are six more ordered water molecules in the region around the carboxylate group of palmitate in the complex. The hydrocarbon chain of the bound palmitate is bent at two places: between atoms C7 and C8 and between atoms C2 and C4. In contrast, fatty acids in complex with human muscle fatty acid binding proteins are more severely bent and adopt a U-shaped conformation [24].

Because the tunnel-like hydrophobic cavity is only large enough to accommodate a single acyl chain, binding of a phospholipid with two fatty acyl chains will mean that one will have to extend into the solvent, where it will be free to adopt multiple conformations. Although this is a thermodynamically unfavorable situation, a similar mode of phospholipid binding has been proposed for *Candida rugosa* lipase, which also has a hydrophobic tunnel [25].

Table 1. Conformation of bound palmitate and its interaction with side chains and solvent.

Atom	Torsion angle (°)	Bond length (Å)	Refined B-factors (Å²)	Side chains and solvent molecules located within 4.5 Å of palmitate
Oε1			36.9	R46, I79, P80, Y81, Sol152, Sol196, Sol197
Oε2			33.6	R46, Y81, V92, Sol152
C1	−179	1.53	32.1	R46, I79, Y81, Sol152, Sol197
C2	−84	1.54	32.4	N37, A40, R46, I79, Sol174, Sol197
C3	−65	1.53	30.5	A40, R46, A49
C4	177	1.52	27.8	A49, L53, Y81
C5	−143	1.51	25.3	L36, N37, I79
C6	154	1.52	27.8	L36, L53
C7	62	1.53	25.4	V33, V77, I79
C8	166	1.52	25.4	V33, P72, I79
C9	−175	1.53	23.7	V33, L53
C10	−157	1.50	25.8	V33, P72
C11	149	1.51	25.9	I11, V33, I71
C12	−170	1.53	30.5	I71, Sol117
C13	174	1.53	35.9	I11
C14	101	1.53	38.9	I71, Sol117
C15		1.53	41.0	I11
C16			42.8	I15, A18, V60

Comparison with structurally or functionally related proteins

To our knowledge, the structure of maize ns-LTP presents the second example of this novel pattern of protein folding, first observed in the structure of HPS [21,22]. A comparison of the amino acid sequences of maize ns-LTP and HPS shows that 31 of the 80 residues (38.8%) in HPS are identical to the corresponding residues in the maize protein. Although the folding patterns of the two proteins are similar, there are many significant structural differences. In order to compare the structures of uncomplexed maize ns-LTP and HPS, the four disulfide bonds were initially superposed. The main-chain atoms of 35 residues showing an average difference ≤3.5 Å were then superposed to obtain an rms difference of 2.0 Å for these atoms and of 4.3 Å for main-chain atoms of 72 residues (omitting the first eight residues of HPS which are not present in the reported model [21]). As discussed above, the eight conserved cysteine residues show an interesting difference in the pairing of the disulfide bonds. The helix H1 in HPS is a 3_{10}-helix, whereas the equivalent portion of the maize protein is α-helical. The C-terminal region of HPS contains a β-strand, whereas the corresponding region in maize ns-LTP is the flexible loop covering the hydrophobic channel and the maize protein contains a 3_{10}-helix near its C terminus. The most significant difference is the absence of a tunnel-like hydrophobic cavity in HPS, which has instead a

wide cleft covered with hydrophobic residues. The absence of a hydrophobic cavity in the structure of HPS probably excludes the possibility of its binding fatty acids or phospholipids. The biological function of HPS has yet to be established.

Proteins which bind fatty acids or phospholipids and that are functionally related to ns-LTP include animal fatty acid binding proteins [24,26–30], apolipoprotein from *Locusta migratoria* [31], *Escherichia coli* acyl carrier protein [32,33], bovine acyl-CoA binding protein [34], and human Clara cell phospholipid-binding protein [35]. Maize ns-LTP shares neither primary sequence homology nor tertiary structural homology with the above mentioned classes of proteins. Animal fatty acid binding proteins have β-sheet structures and the fatty acid is bound in a large interior cavity that also contains ordered water molecules [29]. The others are α-helical proteins. The crystal structure of apolipoprotein from *Locusta migratoria* consists of five long antiparallel α-helices connected by short loops and it has been proposed that a large structural reorganization involving exposure of the hydrophobic interior is necessary for its binding to a lipid surface [31]. A similar conformational change seems unlikely in our model of maize ns-LTP, unless at least one of the two disulfide bonds, Cys30–Cys75 or Cys50–Cys89, is broken. In *E. coli* acyl carrier protein, an ester bond is formed between Ser36 and the carboxylate of fatty acid and it is plausible that the fatty acyl moiety binds in the hydrophobic cavity formed by three long helices [33]. In the structure of the complex between the acyl-CoA binding protein and palmitoyl-CoA, the palmitoyl part is shielded from the solvent by the polar parts of the bound ligand [34]. Recently, the structure of human Clara cell phospholipid-binding protein, in complex with ligand, revealed that a whole molecule of phospholipid is bound inside a large hydrophobic cavity within the protein [35]. In contrast, the tunnel-like hydrophobic cavity in maize ns-LTP is not large enough to accommodate a whole phospholipid. It is plausible that this interaction of moderate strength may facilitate binding and release of phospholipids in the *in vitro* lipid-transfer process aided by the ns-LTPs.

Biological implications

Numerous lipid-transfer proteins (LTPs) that enhance the exchange or net transfer of lipids between membrane vesicles have been isolated from animals, plants and microorganisms. As membrane biogenesis requires the transport of lipids from their site of synthesis to other cell membranes, LTPs presumably play a role in the intracellular movement of lipids [2,8].

Plant non-specific lipid-transfer proteins (ns-LTPs) are small basic proteins of ~9 kDa with four disulfide bonds. They mediate a net transfer of lipids between donor and acceptor membranes *in vitro* [8]. However, many questions remain unanswered about their *in vivo* functions. The physiological significance of their proposed role in transferring lipids between intracellular membranes has recently been brought into question. Spinach LTP has been found to be present extracellularly and to have a leader peptide sequence — a feature normally associated with secretory proteins [36]. There is growing experimental evidence to suggest that plant ns-LTPs or LTP-like proteins may play a role in a number of different biological functions through their ability to bind and carry lipophilic compounds. For example, an LTP-like protein isolated from the surface wax of broccoli [37] may be involved in the transport of the cuticular components required for the biosynthesis of the surface wax. Sterk *et al.* [38] proposed that carrot ns-LTP may be involved in the supply of cutin monomers for cutin synthesis in the cuticular layer of epidermal cells. It has been suggested that castor bean ns-LTP, through its enhancement of the activity of acyl-coenzyme A (acyl-CoA) oxidase, which catalyzes the rate-limiting step of β-oxidation in peroxisomes, may play a regulatory role in the degradation of storage lipids [16]. It has also been suggested that plant ns-LTPs function as fatty acid and acyl-CoA carrier proteins [13–16]. In maize and barley there is evidence that, in combination with thionins, ns-LTPs protect leaves against bacterial and fungal growth [17].

Here we report the first crystal structure of a plant ns-LTP. The folding topology is similar to that of hydrophobic protein from soybean [21]. However, there are significant structural differences including the disulfide pairing. The present structure of ns-LTP from maize seedlings shows that the protein has a tunnel-like hydrophobic cavity that is large enough to accommodate a single acyl chain of long fatty acids. The fatty acid binding mode has been revealed by the refined model of the protein in complex with palmitate, a putative ligand. Thus this study provides a structural basis for understanding the function of plant ns-LTPs in relation to the transfer and binding of acyl chains, be they part of phospholipids, fatty acids, acyl-CoA, or other acyl group-containing molecules such as cutin monomers.

Materials and methods

Protein purification and crystallization

Crystallization and preliminary X-ray data of uncomplexed maize ns-LTP have been reported [19]. For the uncomplexed structure, neither a fatty acid nor a phospholipid has been intentionally included in the crystallization experiments. The crystal belongs to the orthorhombic space group $P2_12_12_1$ with unit cell dimensions a=24.46 Å, b=49.97 Å and c=69.99 Å. There is one protein molecule in the asymmetric unit. For the complex structure, crystallization was performed as above, except that dipalmitoyl phosphatidylcholine (8 mM) was included in the hanging drop and the concentration of sodium formate in the

reservoir solution was 3.4 M with a final pH of 8.30. The crystal belongs to the same orthorhombic space group, $P2_12_12_1$, with similar unit cell dimensions, a=24.80 Å, b=49.60 Å and c=70.10 Å. The refined model showed the electron density of only one palmitate chain per protein molecule. Therefore, thin-layer chromatography was performed to see if the dipalmitoyl phosphatidylcholine was hydrolyzed under the crystallization conditions. This analysis confirmed the bound ligand to be palmitate instead of dipalmitoyl phosphatidylcholine.

X-ray data collection

X-ray data were collected on a FAST TV-area detector (Enraf-Nonius), using the MADNES software [39]. Graphite-monochromatized CuKα X-rays from a rotating anode generator (Rigaku RU-200), running at 40 kV and 50 mA, were used with a 0.3 mm focus cup and a 0.6 mm collimator. The reflection intensities were obtained by the profile-fitting procedure of Kabsch [40] and the data were scaled by the Fourier scaling program [41] (Table 2).

Structure determination

The structure of uncomplexed maize ns-LTP was determined by multiple isomorphous replacement. Three-dimensional difference Patterson maps were calculated with 14–4 Å data for heavy-atom derivatives and were interpreted for heavy-atom positions with the use of the program HASSP [42] in the CCP4 package [43]. Parameters of heavy atoms were refined and isomorphous replacement phases were calculated using the program MLPHARE (Table 3). Minor heavy-atom sites were located by calculating the cross-phase difference Fourier maps. Some heavy-atom sites were shared among derivatives (Table 3). Using nine derivatives, isomorphous differences alone gave a figure-of-merit of 0.85 for 1899 unique reflections between 14 Å and 3.0 Å. The electron-density map calculated with isomorphous replacement phases clearly showed four α-helices and connecting loops. Inclusion of the derivative Pt11 (Tables 2 and 3) was necessary to obtain an interpretable map. An initial model was built with the published sequence of maize ns-LTP [6], using the graphics program FRODO [44] running on a PS390 Graphics System (Evans and Sutherland). The R-factor of the initial model was 49.7% for 10–3.0 Å data (no sigma cutoff). All refinement calculations were carried out using the program X-PLOR [45]. Initially, rigid-body refinements were carried out using 10–3.0 Å data. Molecular dynamics was then initiated with an energy-minimization procedure to remove bad contacts from the model. After simulated annealing runs, which were performed by the standard slow cooling protocol starting from 3000 K and cooling to 300 K, 120 cycles of energy minimization were followed. Isotropic B-factors were initially set to 15 $Å^2$ and refined in the last stages. Between refinement cycles, the model was rebuilt by manual inspection of the $2F_o-F_c$ Fourier maps. The refined model, accounting for 625 non-hydrogen atoms in all 93 amino acid residues as well as 52 ordered water molecules, has an R-factor of 19.9% for all 6930 unique reflections between 8.0 Å and 1.9 Å (no sigma cutoff). The rms deviations from ideal bond lengths and bond angles are 0.016 Å and 1.98°, respectively. The mean positional error in atomic coordinates is estimated to be between 0.20 Å and 0.25 Å by the Luzzati plot [46]. None of the main-chain dihedral angles of non-glycine residues falls outside the allowed regions of the Ramachandran plot. The plot of B-factors against sequence number is given in Fig. 6a. Average B-factors for the main-chain atoms, side-chain atoms and solvent waters are 19.1 $Å^2$, 23.5 $Å^2$ and 38.0 $Å^2$, respectively. The waters with B-factors lower than 60 $Å^2$ have been included. The four α-helices have B-factors generally lower than other regions.

The refined model of uncomplexed maize ns-LTP excluding solvent molecules was used as the starting model for the refinement of the structure of ns-LTP in complex with palmitate. Since the crystal of the palmitate complex was somewhat non-isomorphous (Table 2), the following steps, along with model rebuilding, were taken to produce the refined model: rigid-body refinement, positional refinement, simulated annealing refinement and inclusion of palmitate and solvent molecules. The R-factor of the initial protein model was 46.1% for 10–3.0 Å data (no sigma cutoff). The refined model, accounting for all residues, one molecule of palmitate, 68 ordered water molecules, and one formate ion has an R-factor of 19.3% for all 7335 unique reflections between 8.0 Å and

Table 2. Data collection and processing statistics.

Data set	Derivative preparation conditions	No. of reflections		Resolution (Å)	Completeness (%)	R_{merge}[a] (%)	R_{iso}[b] (%)
		Total	(Unique)				
Native (uncomplexed)		76774	(7765)	1.9	97.5	3.6	
$Hg(NO_3)_2$	70 mM×40 days	11687	(3892)	2.2	82.1	6.1	30.6
$Hg(SCN)_2$	3 mM×12 days	10798	(3823)	2.2	80.7	4.5	18.2
K_2HgI_4	1 mM×9 days	10688	(3897)	2.2	82.2	5.6	18.0
TMLA	12 mM×19 days	11674	(3939)	2.2	83.1	4.6	28.8
K_2OsO_4	10 mM×58 days	11152	(3832)	2.2	81.1	4.4	17.8
Pt11	15 mM×55 days	10492	(3697)	2.2	78.0	4.6	41.0
Na_2PtCl_6	15 mM×53 days	10980	(3790)	2.2	80.0	4.6	16.9
K_3IrCl_6	20 mM×18 days	11844	(3832)	2.2	82.3	3.9	14.1
$IrCl_3$	10 mM×86 days	10646	(3816)	2.2	80.5	3.8	18.0
Native (complexed)		22364	(7449)	1.8	84.7	3.2	48.4

Abbreviations: TMLA, trimethyllead(II) acetate $(CH_3)_3PbCOOCH_3$; Pt11, diamminedinitroplatinum (IV) $[Pt(NH_3)_2(NO_2)_2]Cl_2$. [a] $R_{merge} = \Sigma_h\Sigma_i|I(h)_i - \langle I(h)\rangle|/\Sigma_h\Sigma_i I(h)_i$, where I(h) is the intensity of reflection h, Σ_h is the sum over all reflections and Σ_i is the sum over the i measurements of reflection h. [b] $R_{iso} = \Sigma_h|F_{PH} - F_P|/\Sigma_h F_P$, where F_P and F_{PH} are the native and derivative structure-factor amplitudes, respectively.

Table 3. Statistics for multiple isomorphous replacement phasing.

Data set	No. of sites	Phasing power[a]	R_{Cullis}[b]	Fractional coordinates			Relative occupancy
				X	Y	Z	
$Hg(NO_3)_2$	3	2.0	0.50	0.972	0.441	0.041	1.00
				0.622	0.439	0.161	0.27
				0.798	0.559	0.174	0.23
$Hg(SCN)_2$	2	1.0	0.73	0.961	0.441	0.041	0.35
				0.377	0.941	0.338	0.11
K_2HgI_4	2	1.3	0.69	0.034	0.148	0.083	0.60
				0.970	0.656	0.383	0.31
TMLA	1	1.4	0.60	0.039	0.146	0.081	0.77
K_2OsO_4	3	0.5	0.92	0.582	0.524	0.117	0.15
				0.581	0.426	0.222	0.13
				0.435	0.468	0.350	0.11
Pt11	3	0.8	0.84	0.445	0.495	0.350	1.00
				0.380	0.478	0.485	0.19
				0.538	0.577	0.479	0.16
Na_2PtCl_6	2	0.8	0.81	0.445	0.483	0.350	0.26
				0.592	0.581	0.053	0.13
K_3IrCl_6	2	0.8	0.83	0.385	0.482	0.487	0.23
				0.588	0.582	0.056	0.13
$IrCl_3$	3	0.9	0.76	0.388	0.482	0.487	0.27
				0.591	0.583	0.055	0.21
				0.918	0.132	0.359	0.15

[a]Phasing power = F_H(calc)/E, where F_H(calc) is the calculated scattering amplitude of the heavy-atom structure, and E is the estimated lack-of-closure error. [b]$R_{Cullis} = \Sigma||F_{PH} \pm F_P| - |F_H||/\Sigma|F_{PH} \pm F_P|$. Phasing power and R_{Cullis} are calculated for 14–3.0 Å data.

1.78 Å (no sigma cutoff). The rms deviations from ideal bond lengths and bond angles are 0.016 Å and 1.78°, respectively. The mean positional error in atomic coordinates is estimated to be ~0.2 Å by the Luzzati plot [46]. None of the main-chain dihedral angles of non-glycine residues falls outside the allowed regions of the Ramachandran plot. Average B-factors are lower than those for the uncomplexed structure: 2.7 $Å^2$ and 18.0 $Å^2$ for the main-chain and side-chain atoms, respectively (Fig. 6b). As in the uncomplexed structure, the four α-helices in the complexed structure have generally lower B-factors than other regions. In addition, the N-terminal part of the C-terminal region in the complex structure (residues 78–81) shows much reduced B-factors, compared with the uncomplexed model (Fig. 6). As in the uncomplexed structure, solvent waters with B-factors lower than 60 $Å^2$ have been included in the model and their average B-factor is 31.0 $Å^2$.

The atomic coordinates (and structure factors) for the uncomplexed protein and for the protein in complex with palmitate have been deposited with the Brookhaven Protein Data Bank [tracking numbers T5918 (T5920) and T5919 (T5921), respectively].

Acknowledgements: We thank the Inter-University Center for Natural Science Research Facilities for providing the X-ray equipment. This work was supported by a grant from the Korea Ministry of Science and Technology. We also thank Prof. David Eisenberg (UCLA) and Dr David R Davies (NIH) for carefully reading the manuscript.

References

1. Crain, R.C. & Zilversmit, D.B. (1980). Two nonspecific phospholipid exchange proteins from beef liver. 1. Purification and characterization. *Biochemistry* **19**, 1433–1439.
2. Rueckert, D.G. & Schmidt, K. (1990). Lipid transfer proteins. *Chem. Phys. Lipids* **56**, 1–20.
3. Westerman, J. & Wirtz, K.W.A. (1985). The primary structure of the nonspecific lipid transfer protein (sterol carrier protein 2) from bovine liver. *Biochem. Biophys. Res. Commun.* **127**, 333–338.
4. Takishima, K., Watanabe, S., Yamada, M., Suga, T. & Mamiya, G. (1988). Amino acid sequences of two nonspecific lipid-transfer proteins from germinated castor bean. *Eur. J. Biochem.* **177**, 241–249.
5. Bouillon, P., Drischel, C., Vergnolle, C., Duranton, H. & Kader, J.-C. (1987). The primary structure of spinach-leaf phospholipid-transfer protein. *Eur. J. Biochem.* **166**, 387–391.
6. Tchang, F., *et al.*, & Kader, J.-C. (1988). Phospholipid transfer protein: full-length cDNA and amino acid sequence in maize. *J. Biol. Chem.* **263**, 16849–16855.
7. Désormeaux, A., Blochet, J.-E., Pézolet, M. & Marion, D. (1992). Amino acid sequence of a non-specific wheat phospholipid transfer protein and its conformation as revealed by infrared and Raman spectroscopy. Role of disulfide bridges and phospholipids in the stabilization of the α-helix structure. *Biochim. Biophys. Acta* **1121**, 137–152.
8. Wirtz, K.W.A. (1991). Phospholipid transfer protein. *Annu. Rev. Biochem.* **60**, 73–99.
9. Bernhard, W.R. & Somerville, C.R. (1989). Coidentity of putative amylase inhibitors from barley and finger millet with phospholipid transfer proteins inferred from amino acid sequence homology. *Arch. Biochem. Biophys.* **269**, 695–697.
10. Campos, F.A.P. & Richardson, M. (1984). The complete amino acid sequence of the α-amylase inhibitor I-2 from seeds of ragi (Indian finger millet, *Eleusine coracana* Gaertn.). *FEBS Lett.* **167**, 221–225.
11. Svensson, B., *et al.*, & Svendsen, I. (1986). A 10 kD barley seed protein homologous with an α-amylase inhibitor from Indian finger millet. *Carlsberg Res. Commun.* **51**, 493–500.
12. Yu, Y.G., Chung, C.H., Fowler, A. & Suh, S.W. (1988). Amino acid sequence of a probable amylase/protease inhibitor from rice seeds. *Arch. Biochem. Biophys.* **265**, 466–475.
13. Rickers, J., Tober, I. & Spener, F. (1984). Purification and binding characteristics of a basic fatty acid binding protein from *Avena sativa* seedlings. *Biochim. Biophys. Acta* **794**, 313–319.
14. Rickers, J., Spener, F. & Kader, J.-C. (1985). A phospholipid transfer protein that binds long-chain fatty acid. *FEBS Lett.* **180**, 29–32.
15. Arondel, V., Vergnolle, C., Tchang, F. & Kader, J.-C. (1990). Bifunctional lipid-transfer: fatty acid-binding proteins in plants. *Mol. Cell. Biochem.* **98**, 49–56.
16. Tsuboi, S., Osafune, T., Tsugeki, R., Nishimura, M. & Yamada, M. (1992). Nonspecific lipid transfer protein in castor bean cotyledon cells: subcellular localization and a possible role in lipid metabolism. *J. Biochem.* **111**, 500–508.
17. Molina, A., Segura, A. & García-Olmedo, F. (1993). Lipid transfer proteins (nsLTPs) from barley and maize leaves are potent inhibitors of bacterial and fungal plant pathogens. *FEBS Lett.* **316**, 119–122.
18. Simorre, J.-P., Caille, A., Marion, D., Marion, D. & Ptak, M. (1991). Two- and three-dimensional ^1H NMR studies of a wheat phospholipid transfer protein: sequential resonance assignments and secondary structure. *Biochemistry* **30**, 11600–11608.
19. Shin, D.H. *et al.*, & Suh, S.W. (1994). Crystallization and preliminary X-ray crystallographic analysis of phospholipid transfer protein from maize seedlings. *Proteins* **19**, 80–83.
20. Richardson, J.S. & Richardson, D.C. (1989). Principles and patterns of protein conformation. In *Prediction of Protein Structure and the Principles of Protein Conformation.* (Fasman, G.D., ed), pp. 1–98, Plenum Press, New York.
21. Baud, F., Pebay-Peyroula, E., Cohen-Addad, C., Odani, S. & Lehmann, M.S. (1993). Crystal structure of hydrophobic protein from soybean; a member of a new cysteine-rich family. *J. Mol. Biol.* **231**, 877–887.
22. Murzin, A.G. (1994). New protein folds. *Curr. Opin. Struct. Biol.* **4**, 441–449.
23. Kleywegt, G.J. & Jones, T.A. (1994). Detection, delineation, measurement and display of cavities in macromolecular structures. *Acta Crystallogr. D* **50**, 178–185.
24. Young, A.C.M., *et al.*, & Sacchettini, J.C. (1994). Structural studies on human muscle fatty acid binding protein at 1.4 Å resolution: binding interactions with three C18 fatty acids. *Structure* **2**, 523–534.
25. Grochulski, P., *et al.*, & Cygler, M. (1994). Analogs of reaction intermediates identify a unique substrate binding site in *Candida rugosa* lipase. *Biochemistry* **33**, 3494–3500.
26. Sacchettini, J.C., Gordon., J.I. & Banaszak, L.J. (1989). Crystal structure of rat intestinal fatty-acid-binding protein: refinement and analysis of the *Escherichia coli*-derived protein with bound palmitate. *J. Mol. Biol.* **208**, 327–339.

27. Xu, Z., Bernlohr, D.A. & Banaszak, L.J. (1992). Crystal structure of recombinant murine adipocyte lipid-binding protein. *Biochemistry* **31**, 3484–3492.
28. Buelt, M.K., Xu, Z., Banaszak, L.J. & Bernlohr, D.A. (1992). Structural and functional characterization of the phosphorylated adipocyte lipid-binding protein (pp15). *Biochemistry* **31**, 3493–3499.
29. Scapin, G., Gordon, J.I. & Sacchettini, J.C. (1992). Refinement of the structure of recombinant rat intestinal fatty acid-binding apoprotein at 1.2 Å resolution. *J. Mol. Biol.* **267**, 4253–4269.
30. Eads, J., Sacchettini, J.C., Kromminga, A. & Gordon, J.I. (1993). *Escherichia coli*-derived rat intestinal fatty acid binding protein with bound myristate at 1.5 Å resolution and I-FABP$^{Arg106 \rightarrow Gln}$ with bound oleate at 1.74 Å resolution. *J. Biol. Chem.* **268**, 26375–26385.
31. Breiter, D.R., *et al.*, & Holden, H.M. (1991). Molecular structure of an apolipoprotein determined at 2.5 Å resolution. *Biochemistry* **30**, 603–608.
32. Kim, Y. & Prestegard, J.H. (1989). A dynamic model for the structure of acyl carrier protein in solution. *Biochemistry* **28**, 8792–8797.
33. Holak, T.A., Nilges, M., Prestegard, J.H., Gronenborn, A.M. & Clore, G.M. (1988). Three-dimensional structure of acyl carrier protein in solution determined by nuclear magnetic resonance and the combined use of dynamical simulated annealing and distance geometry. *Eur. J. Biochem.* **175**, 9–15.
34. Kragelund, B.B., Andersen, K.V., Madsen, J.C., Knudsen, J. & Poulsen, F.M. (1993). Three-dimensional structure of the complex between acyl-coenzyme A binding protein and palmitoyl-coenzyme A. *J. Mol. Biol.* **230**, 1260–1277.
35. Umland, T.C., *et al.*, & Sax, M. (1994). Structure of a human Clara cell phospholipid-binding protein–ligand complex at 1.9 Å resolution. *Nat. Struct. Biol.* **1**, 538–545.
36. Bernhard, W.R., Thoma, S., Botella, J. & Somerville, C.R. (1991). Isolation of a cDNA clone for spinach lipid transfer protein and evidence that the protein is synthesized by the secretory pathway. *Plant Physiol.* **95**, 164–170.
37. Pyee, J., Yu, H. & Kolattukudy, P.E. (1994). Identification of a lipid transfer protein as the major protein in the surface wax of broccoli (*Brassica oleracea*) leaves. *Arch. Biochem. Biophys.* **311**, 460–468.
38. Sterk, P., Booij, H., Schellekens, G.A., Van Kammen, A. & De Vries, S.G. (1991). Cell-specific expression of the carrot EP2 lipid transfer protein gene. *Plant Cell* **3**, 907–921.
39. Messerschmidt, A. & Pflugrath, J.W. (1987). Crystal orientation and X-ray pattern prediction routines for area-detector diffractometer systems in macromolecular crystallography. *J. Appl. Crystallogr.* **20**, 306–315.
40. Kabsch, W. (1988). Evaluation of single-crystal X-ray diffraction data from a position-sensitive detector. *J. Appl. Crystallogr.* **21**, 916–924.
41. Weissman, L. (1982). Strategies for extracting isomorphous and anomalous signals. In *Computational Crystallography.* (Sayre, D., ed), pp. 56–63, Oxford University Press (Clarendon), Oxford.
42. Terwilliger, T.C., Kim, S.-H. & Eisenberg, D. (1987). Generalized method of determining heavy-atom positions using the difference Patterson function. *Acta Crystallogr. A* **43**, 1–5.
43. Collaborative Computational Project, No. 4 (1994). The CCP4 suite: programs for protein crystallography. *Acta Crystallogr. D* **50**, 760–763.
44. Jones, T.A. (1985). Interactive computer graphics: FRODO. *Methods Enzymol.* **115**, 157–171.
45. Brünger, A.T. (1992). *X-PLOR Manual Version 3.1.* Yale University, New Haven, CT.
46. Luzzati, V. (1952). Traitement statistique des erreurs dans la determination des structures cristallines. *Acta Crystallogr.* **5**, 802–810.
47. Kraulis, P.J. (1991). MOLSCRIPT: a program to produce both detailed and schematic plots of protein structures. *J. Appl. Crystallogr.* **24**, 946–950.
48. Laskowski, R.A., MacArthur, M.W., Moss, D.S. & Thornton, J.M. (1993). PROCHECK: a program to check the stereochemical quality of protein structures. *J. Appl. Crystallogr.* **26**, 283–291.
49. Sack, J.S. (1988). CHAIN — a crystallographic modeling program. *J. Mol. Graphics* **6**, 244–245.

Received: **14 Nov 1994**; revisions requested: **1 Dec 1994**; revisions received: **30 Dec 1994**. Accepted: **5 Jan 1995**.